PAPER

Check for updates

A self-powered flexible UV photodetector based on an individual ZnO-amorphous Ga_2O_3 core–shell heterojunction microwire†

Yinzhe Liu,[ab] Kewei Liu, ID *[ab] Jialin Yang,[ab] Zhen Cheng,[ab] Xing Chen,[ab] Yongxue Zhu,[ab] Binghui Li,[ab] Lei Liu ID [ab] and Dezhen Shen*[ab]

Self-powered wide band gap semiconductor ultraviolet (UV) photodetectors based on one-dimensional (1D) micro/nanowires have attracted considerable attention on account of their wide potential applications. Here, amorphous Ga_2O_3 was sputtered onto a ZnO microwire at room temperature using magnetron sputtering to form a self-powered ZnO-amorphous Ga_2O_3 core–shell heterojunction microwire UV photodetector. The low temperature growth process of the Ga_2O_3 shell and its amorphous properties make the core–shell structure have a clear interface and it can maintain excellent performance stability under the condition of stress. The heterojunction device exhibits commendable rectifying properties with a rectification ratio of $\sim$20.7 at ± 2 V. Furthermore, a high peak responsivity of 131.4 mA W^{-1} at 265 nm and a fast response speed of <1 s can be observed at 0 V. Even more interestingly, the photoelectric performance of the device hardly changes under various bending conditions, indicating its potential for flexible applications. Our findings in this work open up a new pathway for the design of flexible, self-powered photodetectors.

Introduction

Ultraviolet (UV) detectors, which transform UV light into electrical signals, are extensively utilized in various sectors, including environmental surveillance, medical applications, and missile tracking.[1–3] With the escalating crisis in energy, the demand for UV photodetectors that are both highly efficient and consume minimal energy is critical. Devices like heterojunction, PN junction, and Schottky detectors can function autonomously without any external bias voltage due to their built-in electric field, offering substantial benefits for the development of advanced self-powered UV photodetectors.[4–7] In particular, self-powered UV photodetectors employing wide-bandgap inorganic semiconductors (*e.g.*, ZnO, Ga_2O_3, GaN) are receiving considerable attention. The advantages of these wide-bandgap semiconductor UV photodetectors include their compact size, robust stability, and intrinsic visible blindness (the obviation of external optical filters).[8–12]

In a variety of cutting-edge applications, the interest in flexible photodetectors is surging, particularly due to their

immense promise for mobile information technologies and wearable optoelectronic instruments. The one-dimensional (1D) micro/nanowire core–shell heterostructure, as a configuration conducive to flexibility, amalgamates the merits of disparate functional materials while retaining the intrinsic advantages of 1D substances, such as superior crystallinity, an extensive surface-to-volume ratio, enhanced sensitivity, and aptness for pliable devices.[13–21] Crucially, when used as a photodetector, this core–shell heterojunction is capable of self-powered operation.[18,21,22] Zinc oxide (ZnO) emerges as a preeminent substance for crafting 1D micro-nano core–shell UV photodetectors, thanks to its broad direct bandgap (E_g = 3.37 eV), substantial absorption coefficient, formidable resistance to radiation, a plethora of micro-nanostructures, and eco-compatibility.[23–28] To date, there has been notable advancement in the creation of one-dimensional core–shell UV photodetectors, particularly using ZnO micro-/nano-wires as the foundational layer coupled with other wide-bandgap semiconductors as the outer layer.[16,18,19,29,30] Typically, β-Ga_2O_3, with a bandgap of $\sim$4.9 eV, is often used to construct core–shell heterostructures with ZnO micro-/nano-wires for self-powered UV photodetection.[16,18,19,30] A high responsivity of 9.7 mA W^{-1} has been achieved at 0 V in a ZnO–Ga_2O_3 core–shell heterostructure microwire synthesized *via* a straightforward one-step chemical vapor deposition (CVD) approach.[18] Moreover, it has been demonstrated that the detection could be enhanced by applying certain static strains on the ZnO–Ga_2O_3 core–shell heterojunction microwire through the piezo-phototronic effect.[16] In addition, a fast

a State Key Laboratory of Luminescence and Applications, Changchun Institute of Optics, Fine Mechanics and Physics, Chinese Academy of Sciences, No. 3888 Dongnanhu Road, Changchun, 130033, People's Republic of China. E-mail: liukw@ciomp.ac.cn, shendz@ciomp.ac.cn

b Center of Materials Science and Optoelectronics Engineering, University of the Chinese Academy of Sciences, Beijing 100049, People's Republic of China

This journal is © The Royal Society of Chemistry 2024

J. Mater. Chem. C, 2024, **12**, 9623–9629 | **9623**

Paper

response speed (rise time ∼28.9 µs, fall time ∼85.7 µs) and a high responsivity of 137.9 mA W^{-1} under 254 nm light were observed in a ZnO/Ga$_2$O$_3$ core/shell nanowire array photodetector without an exterior power supply.[30] However, the synthesis temperature for the β-Ga$_2$O$_3$ shell is usually significantly high, which leads to mutual diffusion of the core–shell interface, and then affects its UV photoelectric detection performance.[31–34] Meanwhile, the single-crystal nature of the β-Ga$_2$O$_3$ shell makes the interface properties of ZnO-β-Ga$_2$O$_3$ core–shell wire heterojunctions greatly affected by stress, which limits their application in flexible devices.

Recently, amorphous Ga$_2$O$_3$ (a-Ga$_2$O$_3$) materials have risen to prominence in the field of UV photodetection, lauded for their exceptional photoelectric properties, the feasibility of low-temperature growth, and the absence of the requirement for lattice-matched substrates.[35–39] Therefore, the integration of a-Ga$_2$O$_3$ instead of β-Ga$_2$O$_3$ into ZnO-Ga$_2$O$_3$ core–shell heterostructures is expected to address the challenge of high-temperature mutual diffusion between the shell and ZnO core and flexible application ability. In this study, we employed magnetron sputtering to deposit a-Ga$_2$O$_3$ onto ZnO microwires grown *via* chemical vapor deposition, to construct a self-powered ZnO-a-Ga$_2$O$_3$ core–shell heterojunction microwire UV photodetector. The interface between a-Ga$_2$O$_3$ and ZnO is distinctly sharp, endowing the device with commendable rectifying behavior and photoresponse capabilities even without an applied bias voltage. Notably, the device's photoelectric performance remains consistent under flexed conditions. These experimental outcomes offer valuable perspectives for the development of straightforward, economical, flexible, and self-powered UV photodetectors, with promising implications for portable and wearable electronic applications.

Experimental section

Preparation of ZnO microwires

ZnO microwires were fabricated through a simple chemical vapor deposition (CVD) technique utilizing a blend of ZnO powders and graphite powders in a 1 : 1 weight ratio as the reactant source material. The powder mixture was put into an alumina boat with a clean silicon (Si) chip as the substrate over the powder. Then, the alumina boat was placed in the center of the tube furnace. The boat's temperature was raised to 1030 °C with a heating rate of 10 °C per minute and maintained for 60 minutes, promoting the synthesis of ZnO microwires. Argon (Ar, 4N purity) and oxygen (O$_2$, 5N purity) served as the carrier and oxidizing gases, with flow rates of 100 sccm and 10 sccm, respectively. Upon completion of the growth process, the furnace underwent a natural cooling phase down to ambient temperature (25 °C), during which it was consistently flushed with oxygen and argon gases.

Fabrication of the device

Fig. 1 delineates the fabrication schematic of the ZnO-a-Ga$_2$O$_3$ core–shell heterojunction microwire photodetectors. A ZnO microwire grown by the CVD method was picked up from the boat using a sharp tweezer, and then placed on a flexible polyethylene terephthalate (PET) substrate. The electrode of ZnO was formed by depositing indium at one end of the microwire, followed by a heat treatment at 200 °C to ensure an optimal ohmic contact. The microwire was then masked using adhesive tape. In the subsequent stage, a-Ga$_2$O$_3$ was sputtered onto the microwire to form a ZnO-a-Ga$_2$O$_3$ core–shell heterostructure at ambient temperature (25 °C) and a pressure of 0.5 Pa. The sputtering process was performed at 100 W for an hour using high-purity Ga$_2$O$_3$ ceramic and Ar gas as the target and sputtering gas, respectively. After finishing the sputtering procedure, the mask tape was removed and the indium electrode was prepared on a-Ga$_2$O$_3$ shell. Finally, the device was annealed at 200 °C to ensure an optimal ohmic contact while eliminating the stress on the microwire caused by indium electrodes on both sides.

Characterization of the materials and devices

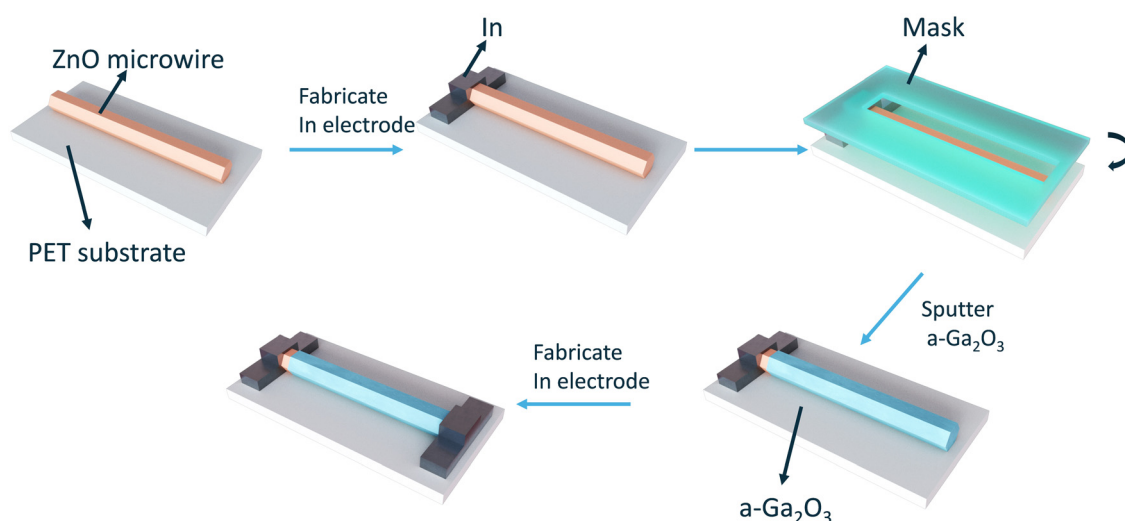The morphology of the samples and elemental composition were characterized by a scanning electron microscope (SEM,

Fig. 1 Schematic fabrication process of the ZnO-Ga$_2$O$_3$ core−shell heterojunction microwire photodetector.

Hitachi S-4800) combined with an energy dispersive spectrometer (EDS). And the crystalline structure was tested by X-ray diffraction (XRD, Bruker D8GADDS). The current–voltage (I–V) and time-dependent current (I–t) characteristics of the device were measured using a semiconductor device analyzer (Agilent B1500A).

Results and discussion

The analytical characterization was conducted on ZnO microwires synthesized via CVD and Ga_2O_3 films deposited through magnetron sputtering onto c-Al_2O_3 substrates. As depicted in Fig. 2(a), the SEM image of an individual ZnO microwire exhibits a hexagonal prism structure with an estimated diameter of ~10 μm, and a notably smooth flat surface. The XRD spectrum presented in Fig. 2(b) displays distinct diffraction peaks at 2θ = 32°, 34.7°, 36.5°, and 47.8°, corresponding to the (100), (002), (101), and (102) crystal planes of the wurtzite ZnO structure, respectively. Additional XRD analysis of the Ga_2O_3 film is illustrated in Fig. 2(c). Aside from the (0006) diffraction peak of the c-Al_2O_3 substrate at 41.8°, the absence of other diffraction peaks suggests the amorphous nature of the Ga_2O_3 film. The optical transmission spectrum, shown in Fig. 2(d), indicates a bandgap of approximately 4.9 eV for the synthesized a-Ga_2O_3.

The cross-sectional SEM image presented in Fig. 3(a) reveals the core–shell architecture of our ZnO-Ga_2O_3 microwire. And
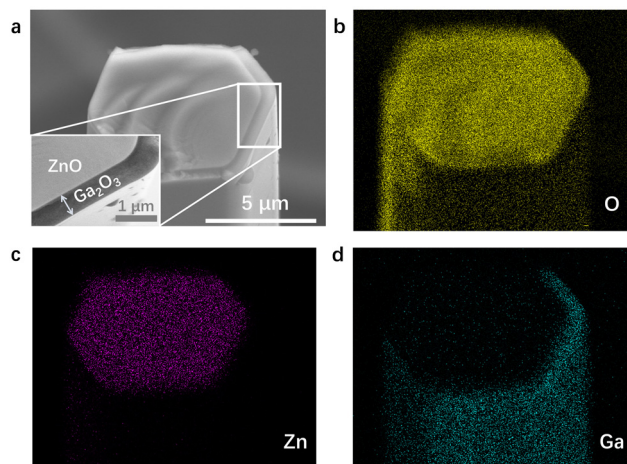

Fig. 3 (a) Cross-sectional SEM image of the ZnO-Ga_2O_3 core–shell microwire. Cross-section EDS mapping images of O (b), Zn (c), and Ga (d).

the well-defined demarcation interface between the core and shell layers is distinctly depicted, and it can be clearly seen that the Ga_2O_3 shell on one side of the ZnO core is about 500 nm thick, and the other side is only tens of nanometres, which is mainly determined by the orientation of the sputtering. The elemental distribution within the ZnO-a-Ga_2O_3 core–shell microwire is elucidated in Fig. 3(b)–(d) through cross-sectional EDS maps. These images confirm the predominant localization of Ga within the shell, Zn within the core, and oxygen (O) across both layers.
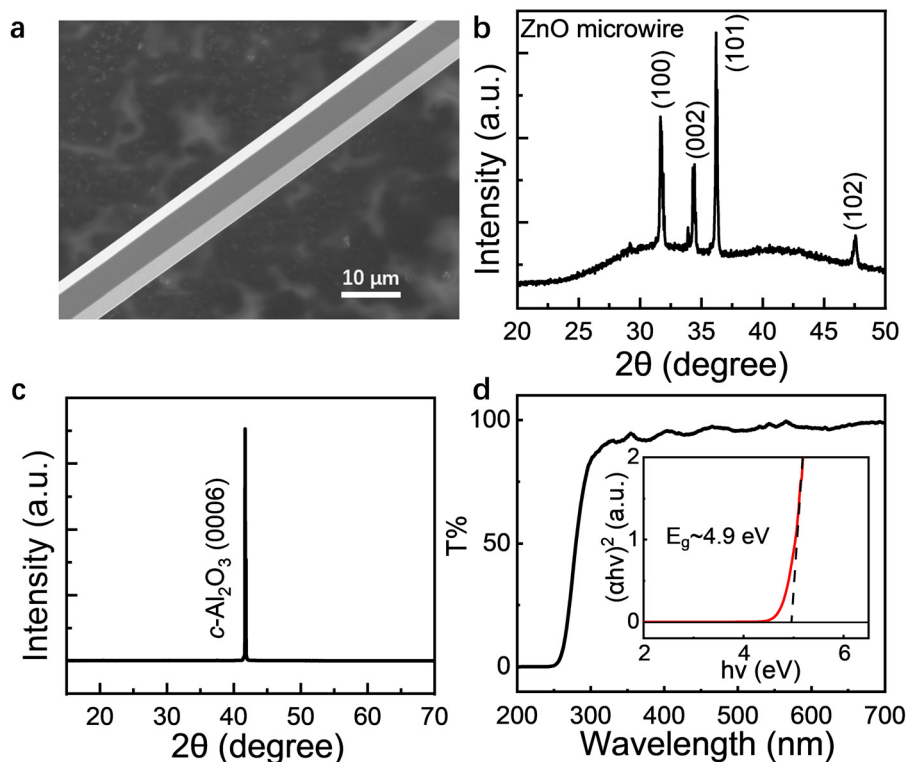

Fig. 2 (a) SEM image of a single ZnO microwire. (b) XRD of ZnO microwires. (c) XRD and (d) transmission spectrum of the a-Ga_2O_3 film on c-Al_2O_3.
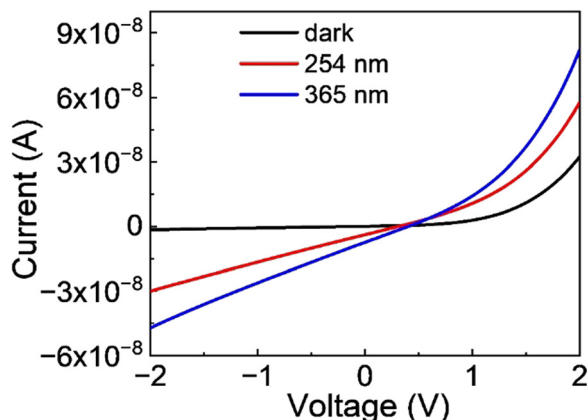
Fig. 4 *I–V* characteristics of the ZnO-a-Ga$_2$O$_3$ core–shell microwire photodetector.

To assess the photodetection capabilities of the ZnO-a-Ga$_2$O$_3$ core–shell microwire, Fig. 4 presents the *I-V* characteristics of the device under dark conditions, as well as under UV illumination at wavelengths of 254 nm ($\sim$0.7 mW cm^{-2}) and 365 nm ($\sim$2 mW cm^{-2}). The device demonstrates significant rectifying behavior with higher current value in the positive voltage region (positive potential on ZnO with respect to Ga$_2$O$_3$) than in the negative voltage region, with a rectification ratio of $\sim$20.7 at $\pm$2 V in the dark. Moreover, under UV light illumination, a substantial increase in current is observed, denoting a robust photoresponse ability of the core–shell microwire photodetector.

To validate the operational efficacy of the ZnO-a-Ga$_2$O$_3$ core–shell microwire photodetector in the absence of an external

bias voltage, we conducted periodic evaluations of the device's *I–t* characteristics at 0 V. A UV lamp at wavelengths of 254 nm (0.7 mW cm^{-2}) and 365 nm (2 mW cm^{-2}) was selected as the light source, as illustrated in Fig. 5(a) and (b), respectively. Observations revealed a swift surge in current upon UV exposure and stabilizing shortly thereafter. Conversely, the cessation of UV illumination resulted in a rapid reversion of current to baseline levels, underscoring the device's remarkable stability and consistent UV detection performance. The normalized enlarged decay edges indicated decay times (defined as the interval for photocurrent reduction from 90% to 10% of peak value) of approximately 0.56 s under 254 nm illumination (Fig. 5(c)) and 0.65 s under 365 nm illumination (Fig. 5(d)). These findings affirm that the device has excellent UV response characteristics, fast response speed and good stability in self-powered operation mode. In addition, the device also exhibits excellent UV photodetection capability under a reverse bias of −2 V, as depicted in Fig. S1 (ESI†).

Fig. 6(a) illustrates the power density dependence (from 0.25 mW cm^{-2} to 2 mW cm^{-2}) of the photocurrent of the photodetector under 254 nm and 365 nm UV illumination at 0 V bias. The photocurrent demonstrates a direct correlation with the intensity of the incident light. The responsivity, a pivotal metric for gauging a photodetector's photoelectric conversion efficiency, is defined as the quotient of the photocurrent (I_{ph}) to the incident optical power (P). This relationship is quantified by the equation:

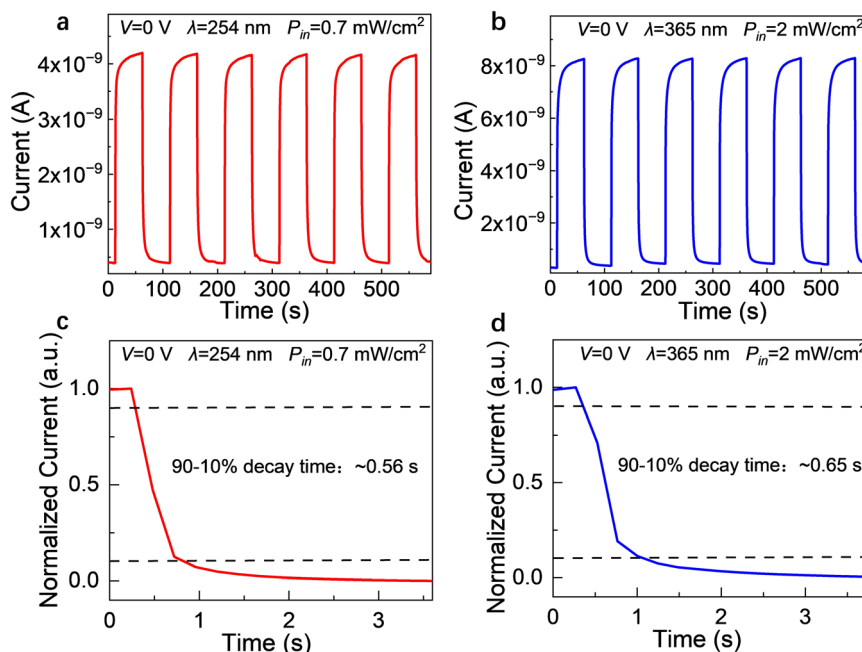$$R = \frac{I_{ph}}{P} = \frac{I_{light} - I_{dark}}{P_{in} \cdot S_{eff}}$$

Fig. 5 *I–t* curves of the ZnO-a-Ga$_2$O$_3$ core–shell microwire under (a) 254 nm light illumination and (b) 365 nm light illumination at 0 V. The normalized photocurrent decay edges under (c) 254 nm light illumination from the enlarged curve in (a) and (d) 365 nm light illumination from the enlarged curve in (b) at 0 V.
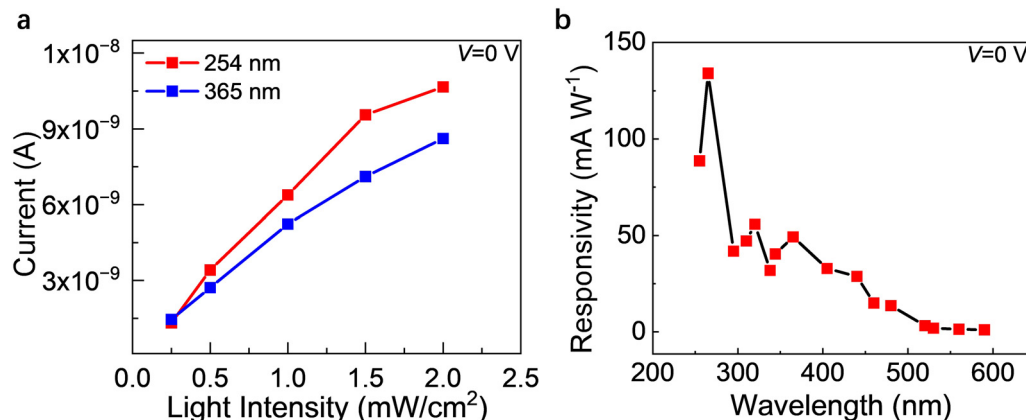
9626 | *J. Mater. Chem. C*, 2024, **12**, 9623–9629

This journal is © The Royal Society of Chemistry 2024

Fig. 6 (a) The photocurrent of the device at 0 V under UV illumination with different power densities. (b) The photoresponse spectrum of the ZnO-a-Ga$_2$O$_3$ core−shell microwire UV photodetector at 0 V.

Here, I_{light} denotes the total current output under illumination, I_{dark} represents the dark current in the absence of light, P_{in} is the power density of the incident light, and S_{eff} is the effective illuminated area of the device ($\sim 8 \times 10^{-5}$ cm^2). The responsivity of our device at 0 V was around 88.7 mA W^{-1} and 49.3 mA W^{-1} under 254 nm and 365 nm illuminations. The difference in responsivity is likely caused by the heterojunction band offset.[40]

Fig. 6(b) showcases the photoresponse spectrum of the ZnO-a-Ga$_2$O$_3$ core−shell heterojunction microwire UV photodetector operating at 0 V. The detector features a peak response at 265 nm, with a responsivity of approximately 134.1 mA W^{-1}. In addition, the 90–10% decay time at 265 nm is 0.46 s (Fig. S2, ESI†). The UV-to-visible rejection ratio (R_{265nm}/R_{600nm}) of our

device surpasses two orders of magnitude, indicating its high selectivity for UV over visible light.

To verify the device in flexible applications, a bending test was performed on the ZnO-a-Ga$_2$O$_3$ core−shell microwire photodetector by varying the bending angles. The schematic diagram and physical image for the bending test is shown in Fig. 7(a). Here, the bending angle θ was defined as the side angle between the two tangents of two electrodes of the device, which can be achieved by controlling the two binder clips. The I–t curves of the device with different bending angles (from 0° to 50° and back to 0°) at 0 V under 254 nm and 365 nm light illumination are shown in Fig. 7(b) and (c), respectively. The negligible variation for normalized I–t performance with different bending conditions can be clearly
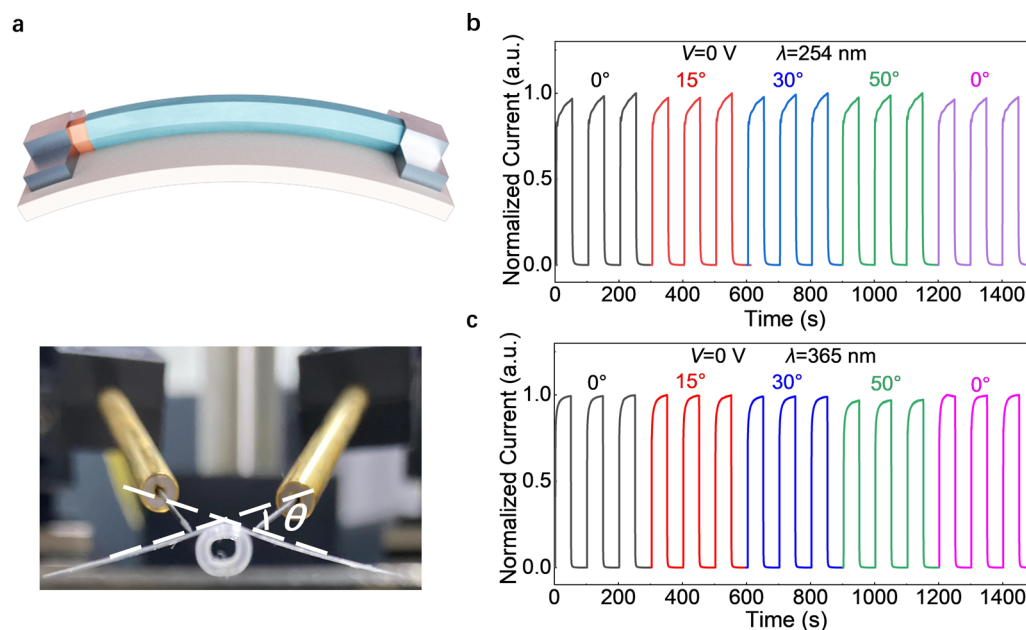

Fig. 7 (a) The schematic diagram and physical image of the bending test. The normalized I–t curves of the flexible ZnO-a-Ga$_2$O$_3$ core-shell microwire photodetector under (b) 254 nm and (c) 365 nm illuminations at 0 V bias with different bending conditions.
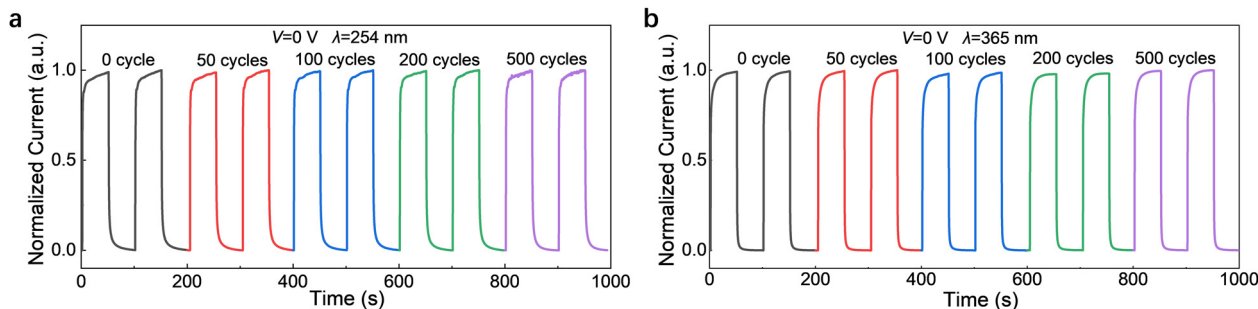
This journal is © The Royal Society of Chemistry 2024

J. Mater. Chem. C, 2024, **12**, 9623–9629 | **9627**

Fig. 8 The normalized I–t curves of the flexible ZnO-a-Ga$_2$O$_3$ core−shell microwire photodetector under (a) 254 nm and (b) 365 nm illuminations at 0 V bias after different bending cycles.

Table 1 A comparison between single ZnO microwire core−shell photodetectors in this work and other works

Photodetector	Responsivity (mA W^{-1})	Decay time	Flexible	Ref.
CH$_3$NH$_3$PbCl$_3$/ZnO	1.769×10^4 (−6 V)@370 nm	500 μs	—	17
β-Ga$_2$O$_3$/ZnO	9.7 (0 V)@251 nm	900 μs	—	18
β-Ga$_2$O$_3$/ZnO	1.3×10^6 (−6 V)@254 nm	42 μs	—	19
Polyaniline/ZnO	60 (−1 V)@365 nm	0.42 s	Yes	20
PEDOT:PSS/ZnO:Ga	185 (0 V)@370 nm	387 μs	—	21
PANI/ZnO	0.56 (0 V)@355 nm	1.45 ms	—	22
ZnO-a-Ga$_2$O$_3$	88.7 (0 V)@254 nm	0.56 s	Yes	This work
	131.4 (0 V)@265 nm	0.46 s		
	49.3 (0 V)@365 nm	0.65 s		

observed, affirming its potential for flexible device applications.

To investigate the stability of the device, the fatigue measurements of the device were tested after different bending cycles. Fig. 8(a) and (b) shows the I–t curves under 254 nm and 365 nm UV light illuminations after 0, 50, 100, 200, and 500 bending cycles, respectively. No obvious change can be observed after 500 bending cycles, which demonstrates that the device has broad application prospects in the field of flexible optoelectronics.

A comprehensive comparative analysis of various core–shell UV photodetectors based on a single ZnO microwire is encapsulated in Table 1. The device delineated in this study demonstrates superior responsivity to UV light at a 0 V bias. Additionally, it maintains excellent photoelectric detection performance in various bending states, indicating its high suitability for flexible applications.

Conclusions

In conclusion, ZnO microwires were fabricated *via* CVD, and a subsequent layer of a-Ga$_2$O$_3$ was deposited through magnetron sputtering to construct a ZnO-a-Ga$_2$O$_3$ core–shell heterojunction microwire UV photodetector. The room-temperature sputtering process effectively reduced interlayer diffusion, and the amorphous nature of the a-Ga$_2$O$_3$ shell enables the device to maintain excellent performance under stress. The device showcased commendable rectifying properties and photoelectric responses, with short decay times of ∼0.56 s and ∼0.65 s at 254 nm and 365 nm,

respectively. Notably, the device achieved a peak responsivity of 131.4 mA W^{-1} at 265 nm at 0 V and demonstrated consistent performance under various bending scenarios, underscoring its versatility for self-powered, wearable, and flexible electronic applications. This work provides new insights for the design of low-power consumption flexible optoelectronic devices.

Author contributions

The manuscript was written through contributions of all authors. All authors have given approval to the final version of the manuscript.

Conflicts of interest

The authors declare no competing financial interest.

Acknowledgements

9628 | *J. Mater. Chem. C*, 2024, **12**, 9623–9629

This journal is © The Royal Society of Chemistry 2024

and Jilin Province Young and Middle-Aged Science and Technology Innovation Leaders and Team Project (20220508153RC).

References

1 K. Liu, M. Sakurai and M. Aono, *Sensors*, 2010, **10**, 8604–8634.

2 J. L. Yang, K. W. Liu, X. Chen and D. Z. Shen, *Prog. Quantum Electron.*, 2022, **83**, 100397.

3 M. Higashiwaki, R. Kaplar, J. Pernot and H. P. Zhao, *Appl. Phys. Lett.*, 2021, **118**, 200401.

4 D. Han, K. Liu, X. Chen, B. Li, T. Zhai, L. Liu and D. Shen, *Appl. Phys. Lett.*, 2021, **118**, 251101.

5 Y. Zhu, K. Liu, X. Huang, P. Zhang, Q. Ai, Z. Cheng, J. Yang, X. Chen, B. Li, L. Liu and D. Shen, *IEEE Electron Device Lett.*, 2023, **44**, 737–740.

6 Y. Zeng, H. Huang, X. L. Zhao, M. F. Ding, X. H. Hou, Y. N. Zou, J. H. Du, J. Y. Liu, S. J. Yu, K. J. Han, Y. H. Wu, X. Z. Zhou, G. W. Xu and S. B. Long, *IEEE Electron Device Lett.*, 2023, **44**, 2003–2006.

7 D. Y. Han, K. W. Liu, Q. C. Hou, X. Chen, J. L. Yang, B. H. Li, Z. Z. Zhang, L. Liu and D. Z. Shen, *Sens. Actuators, A*, 2020, **315**, 112354.

8 C. Zhang, K. W. Liu, Q. Ai, X. Sun, X. Chen, J. L. Yang, Y. X. Zhu, Z. Cheng, B. H. Li, L. Liu and D. Z. Shen, *Mater. Today Phys.*, 2023, **33**, 101034.

9 X. Sun, K. W. Liu, X. Chen, Y. X. Zhu, Z. Cheng, J. L. Yang, B. H. Li, L. Liu and D. Z. Shen, *J. Mater. Chem. C*, 2023, **12**, 118–124.

10 Y. X. Zhu, K. W. Liu, X. Wang, J. L. Yang, X. Chen, X. H. Xie, B. H. Li and D. Z. Shen, *J. Mater. Chem. C*, 2017, **5**, 7598–7603.

11 H. Y. Chen, K. W. Liu, L. F. Hu, A. A. Al-Ghamdi and X. S. Fang, *Mater. Today*, 2015, **18**, 493–502.

12 S. Mauthe, Y. Baumgartner, M. Sousa, Q. Ding, M. D. Rossell, A. Schenk, L. Czornomaz and K. E. Moselund, *Nat. Commun.*, 2020, **11**, 4565.

13 R. Yan, D. Gargas and P. Yang, *Nat. Photonics*, 2009, **3**, 569–576.

14 C. Jia, Z. Lin, Y. Huang and X. Duan, *Chem. Rev.*, 2019, **119**, 9074–9135.

15 X. Liu, L. Gu, Q. Zhang, J. Wu, Y. Long and Z. Fan, *Nat. Commun.*, 2014, **5**, 4007.

16 M. Chen, B. Zhao, G. Hu, X. Fang, H. Wang, L. Wang, J. Luo, X. Han, X. Wang, C. Pan and Z. L. Wang, *Adv. Funct. Mater.*, 2018, **28**, 1706379.

17 Z. Cheng, K. Liu, B. Qiao, J. Yang, X. Chen, Q. Ai, Y. Zhu, B. Li, L. Liu and D. Shen, *Phys. Scr.*, 2023, **98**, 035520.

18 B. Zhao, F. Wang, H. Chen, L. Zheng, L. Su, D. Zhao and X. Fang, *Adv. Funct. Mater.*, 2017, **27**, 1700264.

19 B. Zhao, F. Wang, H. Chen, Y. Wang, M. Jiang, X. Fang and D. Zhao, *Nano Lett.*, 2015, **15**, 3988–3993.

20 L. Zhang, P. Wan, T. Xu, C. Kan and M. Jiang, *Opt. Express*, 2021, **29**, 19202–19213.

21 P. Wan, M. Jiang, T. Xu, Y. Liu and C. Kan, *J. Mater. Sci. Technol.*, 2021, **93**, 33–40.

22 Y. H. Chen, L. X. Su, M. M. Jiang and X. S. Fang, *J. Mater. Sci. Technol.*, 2022, **105**, 259–265.

23 J. Dai, C. Xu, X. Xu, J. Guo, J. Li, G. Zhu and Y. Lin, *ACS Appl. Mater. Interfaces*, 2013, **5**, 9344–9348.

24 H. Ma, K. Liu, Z. Cheng, Z. Zheng, Y. Liu, P. Zhang, X. Chen, D. Liu, L. Liu and D. Shen, *J. Alloys Compd.*, 2021, **868**, 159252.

25 D. Kumar, R. Bai, S. Chaudhary and D. K. Pandya, *Mater. Today Energy*, 2017, **6**, 105–114.

26 Z. W. Jin, Q. Zhou, Y. H. Chen, P. Mao, H. Li, H. B. Liu, J. Z. Wang and Y. L. Li, *Adv. Mater.*, 2016, **28**, 3697–3702.

27 W. Tian, C. Zhang, T. Y. Zhai, S. L. Li, X. Wang, J. W. Liu, X. Jie, D. Q. Liu, M. Y. Liao, Y. Koide, D. Golberg and Y. Bando, *Adv. Mater.*, 2014, **26**, 3088–3093.

28 Y. Z. Liu, K. W. Liu, J. L. Yang, Z. Cheng, D. Y. Han, Q. Ai, X. Chen, Y. X. Zhu, B. H. Li, L. Liu and D. Z. Shen, *Chin. Phys. B*, 2022, **31**, 106101.

29 P. Ghamgosar, F. Rigoni, S. You, I. Dobryden, M. G. Kohan, A. L. Pellegrino, I. Concina, N. Almqvist, G. Malandrino and A. Vomiero, *Nano Energy*, 2018, **51**, 308–316.

30 D. T. You, C. X. Xu, J. Zhao, W. Zhang, F. F. Qin, J. P. Chen and Z. L. Shi, *J. Mater. Chem. C*, 2019, **7**, 3056–3063.

31 E. Alarcón-Lladó, S. Estradé, J. D. Prades, F. Hernandez-Ramírez, J. Arbiol, F. Peiró, J. Ibáñez, L. Artús and J. R. Morante, *CrystEngComm*, 2011, **13**, 656–662.

32 S. S. Liu, M. Y. Li, J. B. Zhang, D. Su, Z. Huang, S. Kunwar and J. O. O. Lee, *Nano-Micro Lett.*, 2020, **12**, 114.

33 X. Huang, M. G. Willinger, H. Fan, Z. L. Xie, L. Wang, A. Klein-Hoffmann, F. Girgsdies, C. S. Lee and X. M. Meng, *Nanoscale*, 2014, **6**, 8787–8795.

34 J. Piotrowski, W. Gawron, Z. Orman, J. Pawluczyk, K. Klos, D. Stepien and A. Piotrowski, *Conference on Infrared Technology and Applications XXXVI*, 2010, **7660**, 766031.

35 C. Q. Zhou, K. W. Liu, X. Chen, J. H. Feng, J. L. Yang, Z. Z. Zhang, L. Liu, Y. Xia and D. Z. Shen, *J. Alloys Compd.*, 2020, **840**, 155585.

36 J. Zhang, F. Liu, D. Liu, Y. Yin, M. Wang, Z. Sa, L. Sun, X. Zheng, X. Zhuang, Z. Lv, W. Mu, Z. Jia, Y. Tan, F. Chen and Z.-X. Yang, *Mater. Today Phys.*, 2023, **31**, 100997.

37 H. Zhou, L. Cong, J. Ma, B. Li, M. Chen, H. Xu and Y. Liu, *J. Mater. Chem. C*, 2019, **7**, 13149–13155.

38 Y. Wang, H. Li, J. Cao, J. Shen, Q. Zhang, Y. Yang, Z. Dong, T. Zhou, Y. Zhang, W. Tang and Z. Wu, *ACS Nano*, 2021, **15**, 16654–16663.

39 S. Cui, Z. Mei, Y. Zhang, H. Liang and X. Du, *Adv. Opt. Mater.*, 2017, **5**, 1700454.

40 D. Y. Han, K. W. Liu, J. L. Yang, X. Chen, B. H. Li, L. Liu and D. Z. Shen, *J. Mater. Chem. C*, 2021, **9**, 10013–10019.

This journal is © The Royal Society of Chemistry 2024

J. Mater. Chem. C, 2024, **12**, 9623–9629 | **9629**